



# Drastic modification of low temperature thermoelectric properties of Na-doped $\text{Bi}_2\text{Sr}_{2-x}\text{Na}_x\text{Co}_2\text{O}_y$ ceramics prepared via laser floating zone technique

G. Çetin<sup>1</sup> · B. Özçelik<sup>1</sup> · M. Gürsul<sup>1</sup> · M. A. Madre<sup>2</sup> · A. Sotelo<sup>2</sup> · S. Adachi<sup>3</sup> · Y. Takano<sup>3</sup>

Received: 27 May 2020 / Accepted: 28 July 2020 / Published online: 19 August 2020  
© Springer Science+Business Media, LLC, part of Springer Nature 2020

## Abstract

In this study,  $\text{Bi}_2\text{Sr}_{2-x}\text{Na}_x\text{Co}_2\text{O}_y$  ( $x=0.0, 0.05, 0.075, 0.10, \text{ and } 0.15$ ) ceramic powders have been fabricated via the classical ceramic route, followed by a texturing process through the laser floating zone technique. XRD patterns show the thermoelectric phase as the major one. In addition, Na-substitution reduces the amount of secondary phases, when compared to the pure sample. SEM observations point out that grain orientation is significantly improved when Na-content is increased. Na-substitution reduces electrical resistivity from 35 (in pure samples) to 19.6 m $\Omega$  cm (in Na=0.05 ones) at around room temperature, while Seebeck coefficient is, approximately, twice measured in Na-free. On the other hand, thermal conductivity is slightly lower in undoped samples (0.83 W/K m), when compared to the Na-substituted ones (1.10–1.40 W/K m) at room temperature, due to their lower electrical conductivity. Finally, ZT values are higher when the Na-content is increased, reaching 0.022 at around 400 K.

## 1 Introduction

Research on alternative energy sources is quite popular due to challenges like the decrease of fossil-fuel-based energy sources, increase in energy demand and global warming. Thermoelectric materials have an important place in this kind of research to enable the reuse of waste heat as electrical energy. These materials allow producing electric energy from a temperature gradient when they are integrated into thermoelectric generators formed by p-n legs. The conversion efficiency of these materials can be obtained from the dimensionless figure of merit,  $ZT$ , defined as  $TS^2/\rho\kappa$ , where  $T$  is the absolute temperature,  $S$  Seebeck coefficient,  $\rho$  electrical resistivity, and  $\kappa$  thermal conductivity [1].  $\text{Bi}_2\text{Te}_3$ ,  $\text{PbTe}$  and  $\text{CoSe}_3$  intermetallics are commonly used as thermoelectric materials in commercial modules. However, this

compounds show some important drawbacks such as their low abundance in the earth's crust [2], and their degradation and/or liberation of heavy elements at high temperatures under air [3]. Such problems have caused the emergence of Co-based oxides, which are abundant in earth's crust, stable at high temperatures, and much less toxic. The first discovered member of this CoO-based family,  $\text{Na}_x\text{CoO}_2$ , exhibits large thermoelectric power, breaking the general belief that oxides had poor thermoelectric properties [4]. This work led to the discovery of new layered cobaltites with p-type behavior, such as Ca–Co–O [5], Bi–Ca–Co–O [6], and Bi–Sr–Co–O [7]. In addition, other families as TiO- and MnO-based materials [8, 9] were discovered, exhibiting n-type properties, being the counterpart of p-type ones in thermoelectric modules.

Various crystallographic studies showed that Co-based crystal structure can be described as composed of two different layers, namely  $\text{CdI}_2$ -type  $\text{CoO}_2$  conductive layer and rock salt (RS)  $\text{Bi}_2\text{X}_2\text{O}_4$  ( $X = \text{Ca, Sr and Ba}$ ) insulating layers. These two layers have common  $a$ - and  $c$ -axis lattice parameters with different  $b$ -axis length, which causes a misfit along the  $b$ -direction [10, 11]. This irregularity in the crystal structure causes a high anisotropy in the material as well as in its electrical properties and Seebeck coefficient. In this regard, cation substitution [12–14] or different synthesis techniques [15–18] have been performed

✉ G. Çetin  
gçetin@cu.edu.tr

<sup>1</sup> Department of Physics, Faculty of Sciences and Letters, Çukurova University, 01330 Adana, Turkey

<sup>2</sup> ICMA (CSIC-Universidad de Zaragoza), C/María de Luna 3, 50018 Zaragoza, Spain

<sup>3</sup> National Institute for Materials Science, 1-2-1 Sengen, Tsukuba, Ibaraki 305-0047, Japan

to enhance thermoelectric properties of these materials. Taking into account these previous studies, the aim of this work is investigating the effect of Na substitution for Ca on the microstructure, and thermoelectric and magnetic properties of  $\text{Bi}_2\text{Sr}_2\text{Co}_2\text{O}_y$  prepared by solid state method followed by LFZ texturing.

## 2 Experimental procedure

$\text{Bi}_2\text{Sr}_{2-x}\text{Na}_x\text{Co}_2\text{O}_y$  ( $x=0, 0.05, 0.075, 0.10, \text{ and } 0.15$ ) thermoelectric ceramics were prepared via the conventional solid state method using  $\text{Bi}_2\text{O}_3$ ,  $\text{SrCO}_3$ ,  $\text{Na}_2\text{CO}_3$ , and  $\text{CoO}$  commercial powders. In a first step, they were homogeneously mixed and ball milled for 30 min. at 300 rpm in distilled water media. Then, infrared lamps were used to dry the suspension and manually milled to break the agglomerates. The resulting homogenous mixtures were calcined twice at 750 and 800 °C to decompose  $\text{CO}_2$  from the metallic carbonates and isostatically pressed into cylindrical rods with radius  $\varphi = 2\text{--}3$  mm, and  $\sim 100$  mm length under 200 MPa. These rods were finally used as feed in LFZ system powered with Nd-YAG laser radiation ( $\lambda = 1064$  nm) [19]. The grown speed of all samples has been 30 mm/h, with 3 rpm seed rotation to obtain the cylindrical geometry. At the same time, the feed was oppositely rotated at 15 rpm to obtain a homogeneous molten zone. This process leads to very dense and geometrically homogeneous cylindrical rods with around 2.5 mm diameter. However, due to its incongruent melting, several secondary phases are also formed through LFZ process, besides the thermoelectric phase [20, 21]. Therefore, a final heat treatment at 810 °C for 24 h was applied to reduce the secondary phases content, increasing the thermoelectric phase proportion in the samples. Consequently, all characterizations have been performed on textured and annealed samples.

Structural features have been determined through the powder XRD technique with  $2\theta$  between 5 and 40 degrees. In order to evaluate the microstructure of  $\text{Bi}_2\text{Sr}_{2-x}\text{Na}_x\text{Co}_2\text{O}_y$  samples a field-emission scanning electron microscope (FESEM, Zeiss Merlin), with an attached EDS system, was used. For these observations, longitudinal polished sections of samples were prepared by hot-embedding the fibers into conducting resin, grinded to reach their center, and finally polished with diamond paste. Electrical resistivity ( $\rho$ ), Seebeck coefficient ( $S$ ), and thermal conductivity ( $\kappa$ ) have been simultaneously measured from 4.2 to 390 K in a Quantum Design PPMS system. Figure of Merit,  $ZT (= S^2T/\rho\kappa)$ , was calculated to establish the thermoelectric performances of these samples as a function of temperature and Na content.

## 3 Results and discussion

Powder XRD patterns were acquired at room temperature and illustrated in Fig. 1. Regardless of Na content, all patterns are quite similar and major peaks correspond to the thermoelectric phase. In the graph, plane reflections for the thermoelectric phase have been labeled, and most of them correspond to the (00 $l$ ) planes, in agreement with previously reported data [19, 22]. In addition, small amount of secondary phases, such as  $\text{Bi}_{0.75}\text{Sr}_{0.25}\text{O}_y$ ,  $\text{CoCo}_2\text{O}_4$  (identified as \*, and #, respectively), were observed due to their incongruent melting. Moreover, when Na content is increased, the amount of these phases is decreased, without observing any Na-based phases. Hence, it can be concluded that Na ions are incorporated into the TE phase and do not create different Na-involved phases.

Representative SEM micrographs of samples after the growth process and presented in Fig. 2. They show several contrasts: Black (#1), dark grey (#2), grey (#3), light grey (#4) and white (#5), which have been identified through EDS as Co oxide, Bi poor phase, TE phase ( $\text{Bi}_2\text{Sr}_{2-x}\text{Na}_x\text{Co}_{1.8}\text{O}_y$ ),  $\text{Bi}_2\text{Sr}_2\text{Co}_1\text{O}_x$ , and Bi/Sr rich oxide, respectively. The compositional variation of the thermoelectric phase in the textured annealed samples with the Na nominal substitution is displayed in Table 1. As it can be observed in this table, Na content is slightly lower than the nominal one, probably due to volatilization of  $\text{Na}_2\text{CO}_3$  during the laser texturing process. In general, volatilization of the molten  $\text{Na}_2\text{CO}_3$  is known as one the factors that limit the performance of molten carbonate fuel cells (MCFC), even operating at lower temperatures [23]. On the other hand, it is clear that the

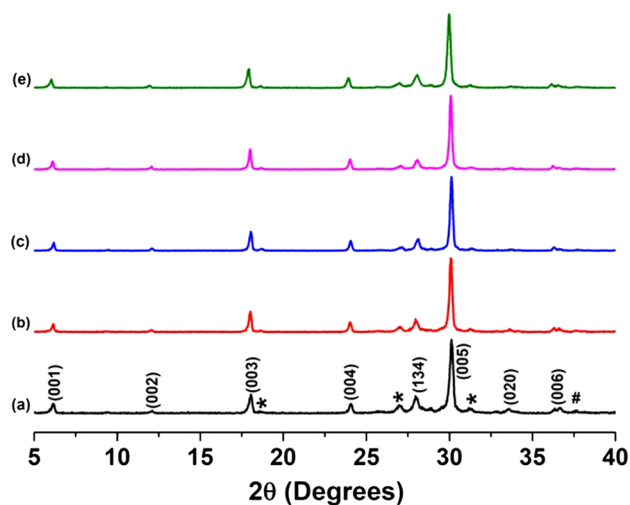


**Fig. 1** XRD patterns of  $\text{Bi}_2\text{Sr}_{2-x}\text{Na}_x\text{Co}_2\text{O}_y$  samples for  $x =$  (a) 0; (b) 0.05; (c) 0.075; (d) 0.10 and (e) 0.15. Diffraction planes identify the peaks associated to the thermoelectric phase, while \* and # correspond to  $\text{Bi}_{0.75}\text{Sr}_{0.25}\text{O}_y$ , and  $\text{CoCo}_2\text{O}_4$  secondary phases, respectively

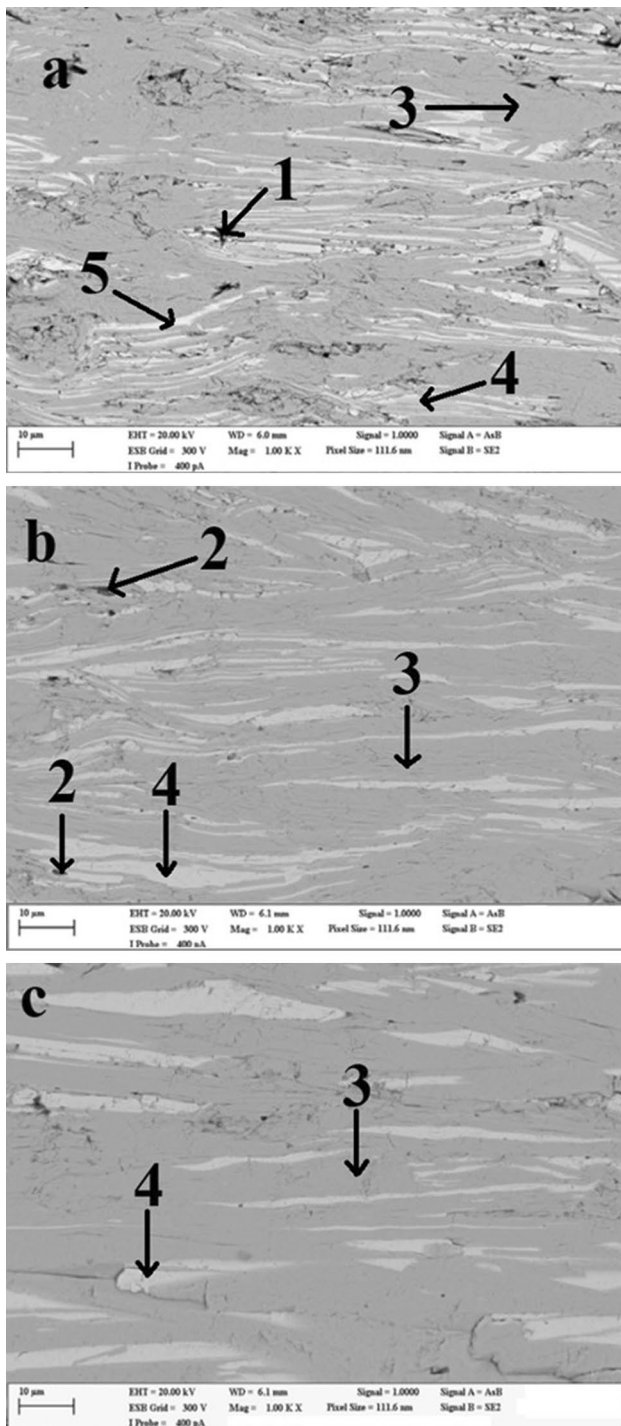


**Fig. 2** Representative SEM micrographs of  $\text{Bi}_2\text{Sr}_{2-x}\text{Na}_x\text{Co}_2\text{O}_y$  samples for  $x =$  (a) 0; (b) 0.075, and (c) 0.15. Black (#1), dark grey (#2), grey (#3), light grey (#4) and white (#5) contrast correspond to Co oxide, Bi poor phase, TE phase ( $\text{Bi}_2\text{Sr}_{2-x}\text{Na}_x\text{Co}_{1.8}\text{O}_y$ ),  $\text{Bi}_2\text{Sr}_2\text{Co}_1\text{O}_x$  and Bi/Sr rich oxide, respectively

secondary phases decrease when the Na content is increased, in agreement with XRD results. Furthermore, with increasing Na-content, better grain orientation is produced, due to

**Table 1** Cationic composition of the thermoelectric phase as a function of the nominal Na substitution obtained through EDS

Nominal Na content	Bi	Sr	Na	Co
0.0	2.0	1.9	0.0	1.8
0.05	2.1	1.8	0.03	1.8
0.075	2.1	1.8	0.06	1.8
0.10	2.0	1.9	0.09	1.8
0.15	2.0	1.8	0.12	1.8

the fact that introducing Na decreases the melting point of the samples, and reduces the radial thermal gradient in the solidification interface, as observed in similar systems [24].

Figure 3 presents electrical resistivity curves between 5 and 390 K for  $\text{Bi}_2\text{Sr}_{2-x}\text{Na}_x\text{Co}_2\text{O}_y$ . At low temperatures, all samples display semiconducting-like behavior ( $dp/dt < 0$ ), reaching the minimum at the metal–insulator-transition-temperature ( $T_{\min}$ ). This transition temperature is increased when the Na content is raised, implying the occurrence of ordering in the incommensurate spin-density-wave (ICSDW) [25]. After this minimum, metallic like behavior is presented ( $dp/dt > 0$ ) up to the so-called  $T^*$  temperature, determining the transition from a strongly correlated Fermi liquid regime to incoherent metal regime [26], and suggesting the existence of mobile carriers.  $T_{\min}$ ,  $T^*$  and room temperature resistivity values are tabulated in Table 2. As it can be seen in the table, the room temperature resistivity of all doped samples is much smaller than those determined in the undoped ones. In addition,  $T_{\min}$  and  $T^*$  values monotonically increase with increasing Na-content. The evolution of these resistivity results can be explained by the reduction of the oxidation state in the rock salt layer provided by the replacement of  $\text{Sr}^{2+}$  with  $\text{Na}^+$ . As a consequence, some  $\text{Co}^{3+}$

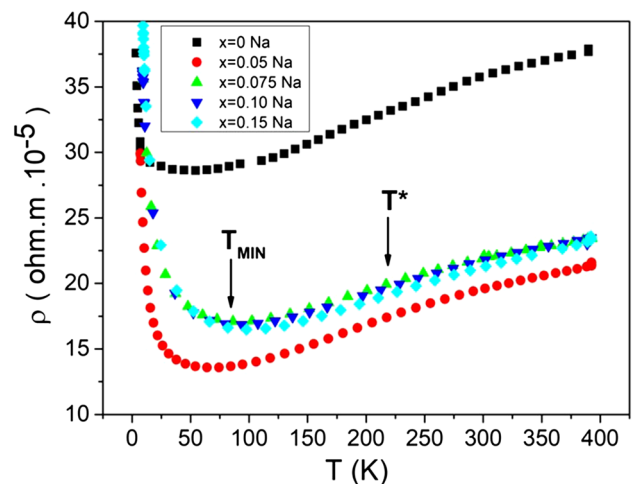


**Fig. 3** Temperature dependence of electrical resistivity for  $\text{Bi}_2\text{Sr}_{2-x}\text{Na}_x\text{Co}_2\text{O}_y$

**Table 2** Electrical and thermal transport parameters for all Bi<sub>2</sub>Sr<sub>2-x</sub>Na<sub>x</sub>Co<sub>2</sub>O<sub>y</sub> samples

Sample	Na=0.00	Na=0.05	Na=0.075	Na=0.10	Na=0.15
T <sub>0</sub> (K)	110 (±0.3)	288 (±0.1)	292 (±0.06)	294 (±0.10)	451 (±0.13)
E <sub>0</sub> (meV)	0.042 (±0.02)	0.55 (±0.07)	0.73 (±0.05)	0.74 (±0.41)	0.84 (±0.26)
T <sub>min</sub> (K)	49 (±4)	74 (±4)	91 (±4)	93 (±4)	97 (±4)
T*	306 (±4)	311 (±4)	353 (±4)	362 (±4)	366 (±4)
κ <sub>ch300K</sub> (WK <sup>-1</sup> m <sup>-1</sup> )	0.02 (±0.001)	0.04 (±0.003)	0.03 (±0.003)	0.03 (±0.003)	0.03 (±0.004)
ρ <sub>300K</sub> (mΩ cm)	35.8 (±0.02)	19.7 (±0.09)	22 (±0.04)	21.9 (±0.03)	21.2 (±0.08)

is raised to Co<sup>4+</sup>, in order to preserve electrical neutrality of the structure, increasing the charge carrier concentration and decreasing resistivity. While room-temperature resistivity value is around 35 mΩ cm for undoped samples, this value decreases to 21.2 mΩ cm for x=0.15 and 19.6 mΩ cm for x=0.05 samples. Variable range hopping (VRH) [16] model can be used at low temperatures to describe the resistivity behavior of samples. In this model, resistivity variation with temperature can be described as:

$$\rho(T) = \rho(0) \exp(T_0/T)^{1/3} \tag{1}$$

where, T<sub>0</sub> is the characteristic temperature of VRH model, given as T<sub>0</sub> = 8/[πk<sub>B</sub>N(ε<sub>F</sub>l<sub>v</sub><sup>2</sup>), in which N(ε<sub>F</sub>) is the density of localized states at Fermi level, k<sub>B</sub> is Boltzmann constant and l<sub>v</sub> is the localization length [27]. T<sub>0</sub> value can be obtained from the slope of lnρ(T) – T<sup>-1/3</sup> graph as shown in Fig. 4a. T<sub>0</sub> values are listed in Table 2, where it can be observed that they increase with increasing Na-content, and implying the decrease of localization length, l<sub>v</sub>.

At higher temperatures, the thermal energy increased, exciting holes carriers, and then VRH model is not sufficient to describe the samples behavior. Instead, thermally activated conduction (TAC) model [26, 27] can be used with the following expression:

$$\frac{1}{\rho} = \mu(T) \exp\left(-\frac{E_0}{k_B}\right) \tag{2}$$

which can be rewritten as;

$$\ln \rho = \frac{E_0}{k_B} T^{-1} - \ln \mu = AT^{-1} + B \tag{3}$$

where μ(T) is charge carriers mobility, k<sub>B</sub> is the Boltzmann constant, E<sub>0</sub> is the energy gap or activation energy due to the spin density wave (SDW) occurring at Fermi surface with fitting parameters A and B. By using this equation, low resistivity data was fitted and presented in Fig. 4b. The slope in the plots of ln ρ versus T<sup>-1</sup> corresponds to the samples activation energy (E<sub>0</sub>). As it can be seen, the obtained E<sub>0</sub> values increase with increasing Na-content, suggesting that replacing Sr with Na positively affects the formation of the SDW propagating in the CoO<sub>2</sub> plane. Furthermore, the increase

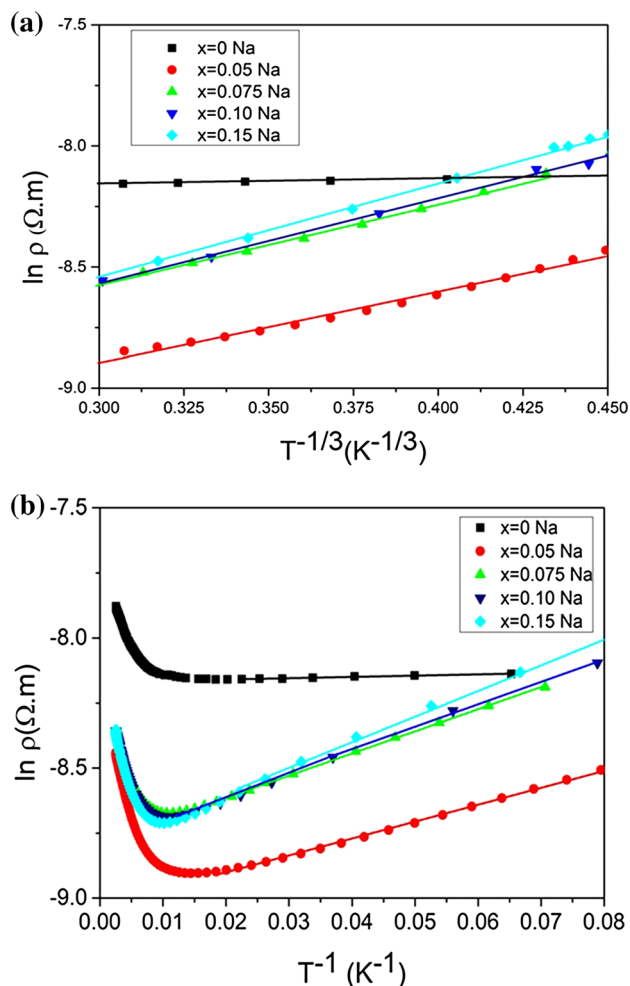


**Fig. 4** a ln ρ – T<sup>-1/3</sup> plots between 10 and 37 K, b ln ρ – T<sup>-1</sup> plots between 12 and 380 K

in the activation energy can be an indication of the Co<sup>3+</sup> to Co<sup>4+</sup> promotions. Hence, introducing Na into the rock salt layer has an indirect effect on the CoO<sub>2</sub> plane promoting SDW state surviving in the CoO<sub>2</sub> plane.

The temperature dependence of Seebeck coefficient as a function of Na-content is presented in Fig. 5. At a first sight, Seebeck coefficient is positive for all samples in the whole measured temperature range which is indicative of p-type conduction. More importantly, Seebeck coefficient

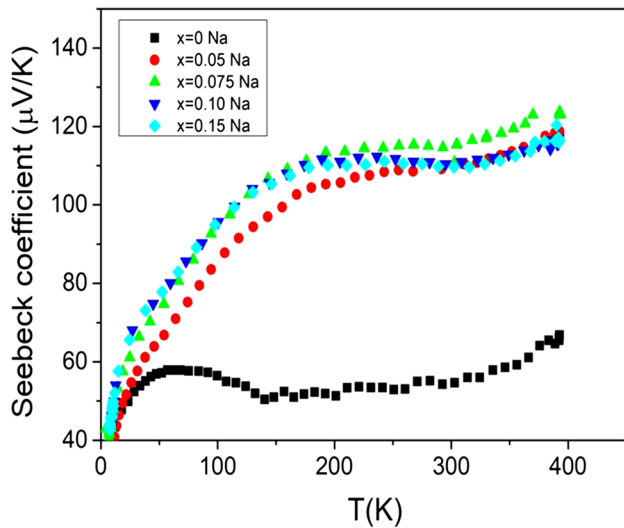


**Fig. 5** Temperature dependence of Seebeck coefficient for  $\text{Bi}_2\text{Sr}_{2-x}\text{Na}_x\text{Co}_2\text{O}_y$

of Na-doped samples is increased, approximately, twice compared to Na-free samples. A temperature-independent expression for the Seebeck coefficient is given by Koshibae et al. [28] as follows;

$$S = -\frac{k_B}{|e|} \ln\left(\frac{1}{6} \frac{x}{1-x}\right) \quad (4)$$

where  $k_B$  is the Boltzmann constant,  $e$  is the electron charge and  $x$  is the concentration of  $\text{Co}^{+4}$  ions. The Seebeck coefficient at room temperature is around  $110 \mu\text{V/K}$  for all Na-doped samples and  $55 \mu\text{V/K}$  for Na-free sample. This Seebeck coefficient increase can be attributed to the higher concentration of  $\text{Co}^{+4}$  ions given in Koshibae's equation. By using this equation, the valence of cobalt ions is approximately 3.45 at around 300 K for Na-doped samples. However, this model is not realistic enough as it is ignoring the peculiar splitting of the  $t_{2g}$  levels in the  $\text{CoO}_2$  layer [29]. As a matter of fact, Seebeck coefficient of Na-doped samples increases almost linearly up to 300 K indicating a temperature dependency. A temperature dependent expression for Seebeck effect is given by the Mott formula [27];

$$S = \frac{C_e}{n} + \frac{T\pi^2 k_B^2}{3e} \left[ \frac{\partial \ln \mu(\epsilon)}{\partial \epsilon} \right] \quad (5)$$

where  $n$ ,  $C_e$ ,  $k_B$  and  $\mu(\epsilon)$  are carrier concentration, electronic specific heat, Boltzmann constant, and energy correlated mobility, respectively. By using this relation, it can be suggested that an increase in carrier concentration reduces Seebeck coefficient as indicated by the first term in Eq. 5. Therefore, the increase in the Seebeck coefficient with Na-content can be explained by the second term in Eq. 5. By increasing

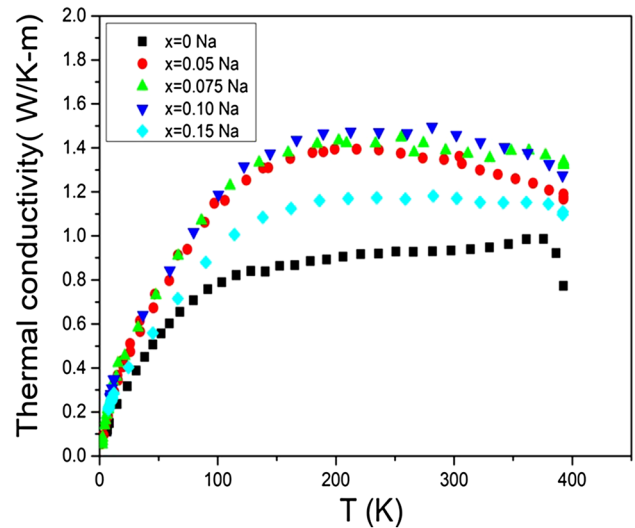


**Fig. 6** Temperature dependence of thermal conductivity for  $\text{Bi}_2\text{Sr}_{2-x}\text{Na}_x\text{Co}_2\text{O}_y$

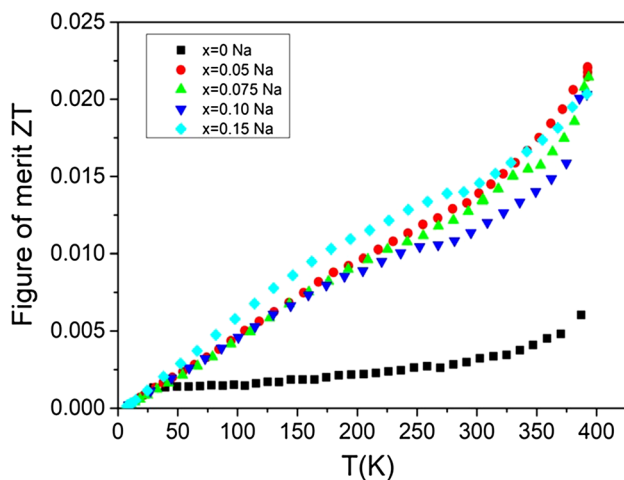
Na-content, due to the disorder arising from Na substitution, the rate of change in the system energy correlated mobility is increased, leading to higher Seebeck coefficient values. At room temperature, the  $S$  values change from 54 (pure samples) to  $115 \mu\text{V/K}$  (0.075 Na doped samples).

Figure 6 presents thermal conductivity,  $\kappa(T)$ , versus temperature curves for the samples. According to the graph, the thermal conductivity behavior of all samples seems very similar. It increases linearly with temperature at low temperatures, and tends to be almost temperature independent at higher ones. Generally, thermal conductivity can be expressed as [30];

$$\kappa(T) = \kappa_{\text{ph}}(T) + \kappa_{\text{ch}}(T) \quad (6)$$

where  $\kappa_{\text{ph}}(T)$  and  $\kappa_{\text{ch}}(T)$  are phonon, and carrier thermal conductivity components, respectively. In this expression  $\kappa_{\text{ch}}(T)$  term can be deduced from Wiedemann–Franz (W–F) law given as  $\kappa_{\text{ch}}(T) = LT/\rho$  where  $L$  is the Lorentz number with the value of  $2.45 \times 10^{-8} \text{ V}^2/\text{K}^2$ . Calculated  $\kappa_{\text{ch}}$  values at room temperature are presented in Table 2. These values are around 0.03 in all cases, being slightly higher for Na doped samples. Typically, the contribution of carrier thermal conductivity component is small, and the main contribution comes from the phonon thermal conductivity component. In addition, the difference between the ionic radii of the Na and Sr affects the lattice vibrations positively by distorting the crystal lattice.

In order to determine TE performances of the samples ZT has been calculated from  $\rho$ ,  $S$  and  $\kappa$  values, and plotted, as a function of temperature, in Fig. 7. Although all Na-substituted samples possess higher thermal conductivity,



**Fig. 7** ZT evolution with respect to temperature for  $\text{Bi}_2\text{Sr}_{2-x}\text{Na}_x\text{Co}_2\text{O}_y$

ZT values of all Na-substituted samples are higher than the obtained in Na-free ones. The largest ZT value has been obtained for  $x=0.15$  sample (0.017) at room temperature. This value is higher than the reported for melt quenched samples (0.010) [31], and in the same order of those obtained in spark plasma textured materials [32].

Temperature dependence of magnetization between 5 and 300 K for all samples is measured. From the results, the magnetization behavior of all samples are found to be quite similar, sharply increasing below 50 K. At higher temperatures, temperature dependence of magnetization is relatively weak and shows a temperature-independent tendency. From Curie Weiss law ( $1/\chi$  versus T graph), the fitting line cuts the temperature axis at negative temperatures. This means that antiferromagnetic-type interactions are dominant at low temperatures [33]. From the magnetic field dependence of magnetization curves for  $\text{BiSr}_{2-x}\text{Na}_x\text{Co}_2\text{O}_y$  fibers under  $\pm 5T$  applied fields at 10 K, it has not been observed any hysteresis behavior.

## 4 Conclusion

In this study,  $\text{Bi}_2\text{Sr}_{2-x}\text{Na}_x\text{Co}_2\text{O}_y$  ceramics were produced via the conventional solid state method and textured using the LFZ technique. XRD patterns showed that major phase is the thermoelectric one regardless of Na concentration. SEM–EDS analysis has shown that Na doping enhances grain orientation and slightly decreases the amount of secondary phases. Samples resistivity is decreased with Na-content, and a broad minimum at  $T_{\min}$  can be observed in all samples, implying the presence IC–SDW ordering. Seebeck coefficient of Na-doped samples increased approximately twice compared to Na-free ones. Although doped samples

possess higher thermal conductivity, due to their lower resistivity and higher Seebeck coefficient, ZT values of all doped samples are higher than for Na-free ones.

**Acknowledgements** This work is supported by Research Fund of Çukurova University, Adana, Turkey, under grant contracts no: FDK-2016-6105 and FBA-2019-12034. M. A. Madre and A. Sotelo wish to thank the Gobierno de Aragón–FEDER (Research Group T 54-17 R), and the Spanish MINECO–FEDER (MAT2017-82183-C3-1-R) for financial support. The use of Servicio General de Apoyo a la Investigación–SAI, Universidad de Zaragoza is also acknowledged.

## References

1. D.M. Rowe, in *Thermoelectrics Handbook: Macro to Nano*, 1st edn., ed. by D.M. Rowe (CRC Press, Boca Raton, 2006), pp. 1–3
2. A.A. Yaroshevsky, Abundances of chemical elements in the Earth's crust. *Geochem. Int.* **44**, 48–55 (2006)
3. M.H. Elsheikh, D.A. Shnawah, M.F.M. Sabri, S.B.M. Said, M.H. Hassan, M.B.A. Bashir, M. Mohamad, A review on thermoelectric renewable energy: principle parameters that affect their performance. *Renew. Sust. Energy Rev.* **30**, 337–355 (2014)
4. I. Terasaki, Y. Sasago, K. Uchinokura, Large thermoelectric power in  $\text{NaCo}_2\text{O}_4$  single crystals. *Phys. Rev. B* **56**, R12685 (1997)
5. S.W. Li, R. Funahashi, I. Matsubara, K. Ueno, H. Yamada, High temperature thermoelectric properties of oxide  $\text{Ca}_9\text{Co}_{12}\text{O}_{28}$ . *J. Mater. Chem.* **9**, 1659 (1999)
6. A. Maignan, S. Hebert, M. Hervieu, C. Michel, D. Pelloquin, D. Khomskii, Magnetoresistance and magnetothermopower properties of  $\text{Bi}/\text{Ca}/\text{Co}/\text{O}$  and  $\text{Bi}(\text{Pb})/\text{Ca}/\text{Co}/\text{O}$  misfit layer cobaltites. *J. Phys. Condens. Matter* **15**, 2711 (2003)
7. R. Funahashi, I. Matsubara, S. Sodeoka, Thermoelectric properties of  $\text{Bi}_2\text{Sr}_2\text{Co}_2\text{O}_x$  polycrystalline materials. *Appl. Phys. Lett.* **76**, 2385 (2000)
8. H. Wang, C.L. Wang, Thermoelectric properties of Yb-doped  $\text{La}_{0.1}\text{Sr}_{0.9}\text{TiO}_3$  ceramics at high temperature. *Ceram. Int.* **39**, 941–946 (2013)
9. Y.H. Zhu, W.B. Su, J. Liu, Y.C. Zhou, J. Li, X. Zhang, Y. Du, C.L. Wang, Effects of Dy and Yb co-doping on thermoelectric properties of  $\text{CaMnO}_3$  ceramics. *Ceram. Int.* **41**, 1535–1539 (2015)
10. Y. Miyazaki, Crystal structure and thermoelectric properties of the misfit-layered cobalt oxides. *Solid State Ion.* **172**, 463 (2004)
11. H. Leligny, D. Grebille, O. Perez, A.C. Masset, M. Hervieu, B. Raveau, A five-dimensional structural investigation of the misfit layer compound  $[\text{Bi}_{0.87}\text{SrO}_2]_2[\text{CoO}_2]_{1.82}$ . *Acta Cryst. B* **56**, 173 (2000)
12. H.S. Hao, Q.L. He, L.M. Zhao, Thermoelectric properties of Cu-substituted  $\text{Bi}_2\text{Ca}_2\text{Co}_2\text{O}_y$  misfit oxides. *Adv. Mater. Res.* **284–286**, 2263 (2011)
13. G. Constantinescu, M.A. Torres, S.H. Rasekh, J.C. Diez, M.A. Madre, A. Sotelo, Effect of Sr substitution for Ca on the  $\text{Ca}_3\text{Co}_4\text{O}_9$  thermoelectric properties. *J. Alloys Compd.* **577**, 511–515 (2013)
14. N. Sun, S.T. Dong, B.B. Zhang, Y.B. Chen, J. Zhou, S.T. Zhang, Z.B. Gu, S.H. Yao, Y.F. Chen, Intrinsically modified thermoelectric performance of alkaline-earth isovalently substituted  $[\text{Bi}_2\text{AE}_2\text{O}_4][\text{CoO}_2]_y$  single crystals. *J. Appl. Phys.* **114**, 043705 (2013)
15. Y. Zhang, J. Zhang, Q. Lu, Synthesis of highly textured  $\text{Ca}_3\text{Co}_4\text{O}_9$  ceramics by spark plasma sintering. *Ceram. Int.* **33**, 1305 (2007)
16. H. Itahara, C. Xia, J. Sugiyama, T. Tani, Fabrication of textured thermoelectric layered cobaltites with various rock salt-type layers by using  $\beta\text{-Co}(\text{OH})_2$  platelets as reactive templates. *J. Mater. Chem.* **14**, 61 (2004)

17. J.G. Noudem, D. Kenfaui, D. Chateigner, M. Gomina, Granular and Lamellar thermoelectric oxides consolidated by spark plasma sintering. *J. Korean Inst. Electr. Electron. Mater. Eng.* **40**, 1100 (2011)
18. N.M. Ferreira, Sh Rasekh, F.M. Costa, M.A. Madre, A. Sotelo, J.C. Diez, M.A. Torres, New method to improve the grain alignment and performance of thermoelectric ceramics. *Mater. Lett.* **83**, 144–147 (2012)
19. A. Sotelo, Sh Rasekh, G. Constantinescu, M.A. Torres, M.A. Madre, J.C. Diez, Improvement of textured  $\text{Bi}_{1.6}\text{Pb}_{0.4}\text{Sr}_2\text{Co}_{1.8}\text{O}_x$  thermoelectric performances by metallic Ag additions. *Ceram. Int.* **39**, 1597–1602 (2013)
20. S.H. Rasekh, F.M. Costa, N.M. Ferreira, M.A. Torres, M.A. Madre, J.C. Diez, A. Sotelo, Use of laser technology to produce high thermoelectric performances in  $\text{Bi}_2\text{Sr}_2\text{Co}_{1.8}\text{O}_x$ . *Mater. Design* **75**, 143 (2015)
21. E. Combe, R. Funahashi, T. Barbier, F. Azough, R. Freer, Decreased thermal conductivity in  $\text{Bi}_2\text{Sr}_2\text{Co}_2\text{O}_x$  bulk materials prepared by partial melting. *J. Mater. Res.* **31**, 1296 (2016)
22. M. Kato, Y. Goto, K. Umehara, K. Hirota, I. Terasaki, Synthesis and physical properties of Bi–Sr–Co–oxides with 2D-triangular Co layers intercalated by iodine. *Phys. B* **378–380**, 1062–1063 (2006)
23. K. Sugiura, M. Yamauchi, K. Tanimoto, Y. Yoshitani, Evaluation of volatile behaviour and the volatilization volume of molten salt in DIR-MCFC by using the image measurement technique. *J. Power Sour.* **145**, 199 (2005)
24. F.M. Costa, N.M. Ferreira, S.H. Rasekh, A.J.S. Fernandes, M.A. Torres, M.A. Madre, J.C. Diez, A. Sotelo, Very large superconducting currents induced by growth tailoring. *Cryst. Growth Des.* **15**, 2094 (2015)
25. J. Sugiyama, H. Itahara, T. Tani, J.H. Brewer, E.J. Ansaldo, Magnetism of layered cobalt oxides investigated by muon spin rotation and relaxation. *Phys. Rev. B* **66**, 134413 (2002)
26. Y. Huang, B. Zhao, R. Ang, S. Lin, Z. Huang, S. Tan, Y. Liu, W. Song, Y. Sun, Enhanced thermoelectric performance and room-temperature spin-state transition of  $\text{Co}^{4+}$  ions in the  $\text{Ca}_3\text{Co}_{4-x}\text{Rh}_x\text{O}_9$  system. *J. Phys. Chem. C* **117**, 11459 (2013)
27. N.F. Mott, E.A. Davis, *Electronic Processes in Non-Crystalline Materials* (Clarendon Press, London, 1971)
28. W. Koshibae, K. Tsuitsui, S. Maekawa, Thermopower in cobalt oxides. *Phys. Rev. B* **62**, 6869 (2000)
29. L.H. Yin, R. Ang, L.J. Li, B.C. Zhao, Y.K. Fu, X.B. Zhu, Z.R. Yang, W.H. Song, Y.P. Sun, Thermoelectric properties of sol–gel derived cobaltite  $\text{Bi}_2\text{Ca}_{2.4}\text{Co}_2\text{O}_y$ . *Phys. B* **406**, 2914 (2011)
30. Y. Wang, Y. Sui, X.J. Wang, W.H. Su, X.Y. Liu, Enhanced high temperature thermoelectric characteristics of transition metals doped  $\text{Ca}_3\text{Co}_4\text{O}_{9+\delta}$  by cold high pressure fabrication. *J. Appl. Phys.* **107**, 033708 (2010)
31. J. Lingner, R. Funahashi, E. Combe, M. Letz, G. Jakob, Thermoelectric sintered glass-ceramics with a  $\text{Bi}_2\text{Sr}_2\text{Co}_2\text{O}_x$  phase. *Appl. Phys. A* **120**, 59 (2015)
32. K. Rubesova, T. Hlasek, V. Jakes, S. Huber, J. Hejtmanek, D. Sedmidubsky, Effect of a powder compaction process on the thermoelectric properties of  $\text{Bi}_2\text{Sr}_2\text{Co}_{1.8}\text{O}_x$  ceramics. *J. Eur. Ceram. Soc.* **35**, 525 (2015)
33. G.Ç. Karakaya, B. Özçelik, M.A. Torres, M.A. Madre, A. Sotelo, Effect of Na-doping on thermoelectric and magnetic performances of textured  $\text{Bi}_2\text{Sr}_2\text{Co}_2\text{O}_y$  ceramics. *J. Eur. Ceram. Soc.* **38**, 515 (2018)

**Publisher's Note** Springer Nature remains neutral with regard to jurisdictional claims in published maps and institutional affiliations.